Computers and Structures 173 (2016) 50–60

Contents lists available at ScienceDirect

Computers and Structures

journal homepage: www.elsevier.com/locate/compstruc

Transient implicit wave propagation dynamics with the method of finite spheres

Ki-Tae Kim, Klaus-Jürgen Bathe *

Department of Mechanical Engineering, Massachusetts Institute of Technology, Cambridge, MA, USA

ARTICLE INFO

Article history:
Received 17 March 2016
Accepted 15 May 2016
Available online 8 June 2016

Keywords:
Wave propagation
Transient solutions
Method of finite spheres
Implicit dynamics
Bathe method

ABSTRACT

In the paper by Ham et al. (2014), the method of finite spheres enriched for transient wave propagation problems was used and a monotonic convergence of the calculated solutions with decreasing time step size was seen. This is an important property for practical analyses and different from what is seen in traditional finite element solutions. In this paper we explicitly show and study this characteristic through a dispersion analysis of the solutions calculated by the method of finite spheres using an implicit time integration method, the Bathe method. Another important property identified is that in uniform spatial discretizations for the problems solved, the calculated solution accuracy is almost independent of the solution direction considered. Numerical solutions of some wave propagation problems are given to demonstrate these attributes and show that with the schemes discussed very accurate response predictions can be obtained.

1. Introduction

In transient wave propagation problems, spatial and temporal discretizations introduce dispersion not present in analytical solutions, and hence this error is referred to as 'numerical dispersion'. The accuracy of numerical solutions can be bad due to this dispersion. When applying numerical methods to wave propagation problems, spatial and temporal discretizations should, therefore, be chosen according to the dispersion properties of the methods used and it is difficult to obtain accurate solutions to complex problems.

The finite element method with direct time integrations has been widely used to solve wave propagation problems. Considerable research efforts have been focused on the dispersion analysis of finite element solutions to the wave or Helmholtz equation [2–9]. The finite element discretization with the consistent mass matrix in general results in a faster phase velocity than the exact propagation velocity, while a lumped mass approximation leads to slower phase velocity [2–5,10]. In addition, the finite element solutions using uniform meshes show numerical anisotropy, i.e., the solution error depends on the direction considered although the exact wave propagation is the same in all directions [4–6,8–10]. The effect of temporal discretizations using various time integration methods on solutions has also been studied [2,3,5,9] with the error giving period elongations and amplitude decays [11,12].

Numerous methods have been proposed to reduce the dispersion error of finite element solutions [5,10,13–19]. However, in general two- and three-dimensional problems, most of these methods suffer from numerical anisotropy and/or are complicated to use. The higher-order finite element method such as the spectral element method [20] can reduce the dispersion error and the numerical anisotropy [21], but it can be difficult to solve two- and three-dimensional problems in practical analyses.

Another approach to improve the finite element solutions of wave propagation problems is based on trying to cancel out opposing effects. The finite element discretization with the consistent mass matrix gives an overestimated phase velocity while the use of the trapezoidal rule results in an underestimated phase velocity, and it is found that the combined effect leads to a decrease in dispersion error [3].

The Bathe method [22,23], an implicit time integration method, was shown to be very effective when used with bi-linear finite elements because the dissipation property of the Bathe method attenuates undesired high frequency waves. At optimal spatial and temporal discretizations for single types of waves, the solutions are almost non-dispersive but show numerical anisotropy [9]. Since the solutions of practical problems contain multiple types of waves, e.g., longitudinal, transverse and surface waves at different wave speeds, the optimality for all wave predictions is lost, and all waves cannot be accurately calculated at the same time.

* Corresponding author.
E-mail address: kjb@mit.edu (K.J. Bathe).

http://dx.doi.org/10.1016/j.compstruc.2016.05.016
0045-7949/

Recently, the method of finite spheres [24–27], a meshless method, was applied to transient wave propagation problems using the Bathe method, and it was found that the method of finite spheres enriched by trigonometric polynomials is very effective for such problems [1]. The computational time was similar to the time used for bi-linear finite element solutions. An interesting observation was that the solution accuracy using the method of finite spheres increases as the time step size decreases. This result is very important in practice because accurate solutions for multiple types of waves can thus be obtained. Another attractive finding is that, in uniform spatial discretizations, the numerical anisotropy was negligible in the method of finite spheres solutions. These findings in numerical solutions suggest that the method of finite spheres enriched by trigonometric polynomials may be more effective than the traditional finite element method for transient wave propagation problems. However, these results were only observed in numerical examples and were not derived from a systematical dispersion analysis.

The objective of this paper is to study the method of finite spheres used with the Bathe time integration method for the solution of transient wave propagation problems. We use the Bathe method for the temporal discretization since it has favorable dispersion and dissipation properties [11]. In the following, we theoretically derive the dispersion properties of the proposed scheme in one- and two-dimensional analyses, and apply the method to some wave propagation problems to illustrate the important results.

2. Dispersion analysis

In this section, we investigate the dispersion properties of solutions to the standard wave equation when using the method of finite spheres with the Bathe time integration. We consider one- and two-dimensional cases, but the same approach can be extended to the three-dimensional case.

The wave equation is given as

$$\frac{\partial^2 u}{\partial t^2} - c^2 \nabla^2 u = 0 \tag{1}$$

where t is time, ∇^2 is the Laplace operator, u is the solution variable and c is the wave propagation velocity. In a fixed Cartesian coordinate system, a basic sinusoidal plane wave solution to Eq. (1) is given by

$$u = A e^{i(k\mathbf{n}\cdot\mathbf{x}-\omega t)} \tag{2}$$

where A is the amplitude of the wave, k is the wavenumber, $\mathbf{n}$ is a unit vector in the direction of wave propagation, $\mathbf{x}$ is a position vector measured from the origin of the coordinate system, ω is the angular frequency and $i = \sqrt{-1}$. If we substitute from Eq. (2) into Eq. (1), we obtain

$$c^2 = \left(\frac{\omega}{k}\right)^2 \tag{3}$$

and the analytical solution is non-dispersive.

In the method of finite spheres, the solution u is approximated as [24–27]

$$u(\mathbf{x}) = \sum_{I=1}^{N} \sum_{m=1}^{n_I} h_{Im}(\mathbf{x}) \alpha_{Im} \tag{4}$$

where N is the number of spheres used for spatial discretization, n_I is the number of local basis functions used in the sphere I, and the shape function h_{Im} associated with the coordinates α_{Im} is

$$h_{Im}(\mathbf{x}) = \varphi_I(\mathbf{x}) p_{Im}(\mathbf{x}) \tag{5}$$

where φ_I and p_{Im} are the partition of unity function and the local basis function which are subordinate to the sphere I, respectively. The partition of unity function is constructed by the Shepard function [28]

$$\varphi_I(\mathbf{x}) = \frac{W_I(\mathbf{x})}{\sum_{J=1}^{N} W_J(\mathbf{x})} \tag{6}$$

where we use the quartic spline function

$$W_I(\mathbf{x}) = W(s_I),$$
$$W(s_I) = \begin{cases} 1 - 6s_I^2 + 8s_I^3 - 3s_I^4 & \text{for } 0 \leqslant s_I < 1, \\ 0 & \text{for } s_I \geqslant 1 \end{cases} \tag{7}$$

with $s_I = \|\mathbf{x} - \mathbf{x}_I\|/r_I$ where $\mathbf{x}_I$ and r_I refer to the center position vector and the radius of the sphere I, respectively.

Then the finite sphere discretization of Eq. (1) yields

$$\mathbf{M}\ddot{\boldsymbol{\alpha}} + c^2 \mathbf{K}\boldsymbol{\alpha} = \mathbf{0} \tag{8}$$

where $\mathbf{M}$, $\mathbf{K}$ and $\boldsymbol{\alpha}$ are the associated "mass" and "stiffness" matrices and the vector of unknown coefficients to be found, respectively. Note that $\mathbf{M}$ is dimensionless and $\mathbf{K}$ has the dimension of $1/\text{length}^2$.

If the Bathe method is applied to Eq. (8) for temporal discretization (see Refs. [22,23] for the detailed formulation of the Bathe method), we obtain the discretized wave equation

$$\left(72\mathbf{M} + 8c^2\Delta t^2 \mathbf{K}\right)^{t+\Delta t}\boldsymbol{\alpha} + \left(-144\mathbf{M} + 5c^2\Delta t^2 \mathbf{K}\right)^{t+\Delta t/2}\boldsymbol{\alpha} + \left(72\mathbf{M} + 5c^2\Delta t^2 \mathbf{K}\right)^{t}\boldsymbol{\alpha} = \mathbf{0} \tag{9}$$

where Δt denotes the time step size.

For the dispersion analysis of the solution to Eq. (9), we uniformly distribute nodes spaced a distance $\Delta x = \Delta y$ apart and use $r_I = \Delta x$ for each sphere I, as shown in Fig. 1. Also, n_p local basis

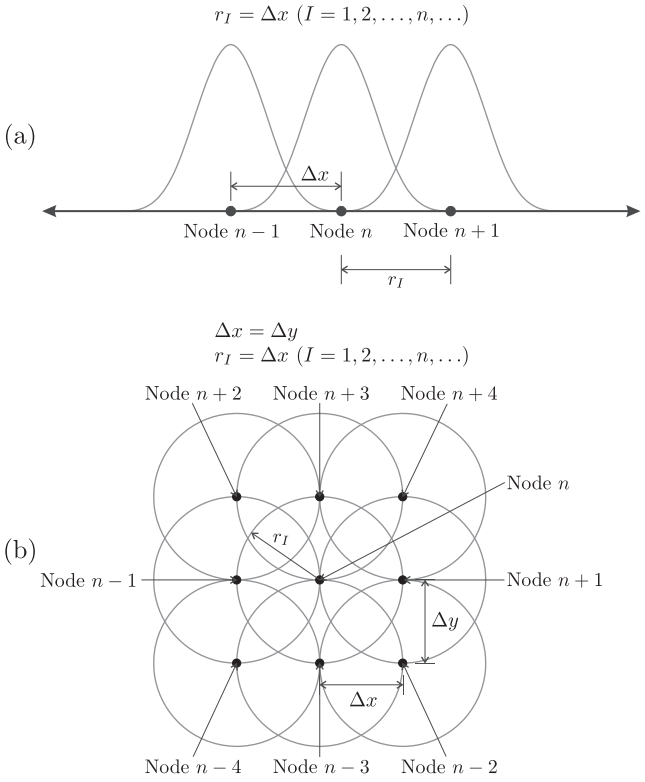

Fig. 1. Uniformly distributed nodes used in the method of finite spheres: (a) one-dimensional case and (b) two-dimensional case.

Table 1
Sets of local basis functions used in the method of finite spheres; $\bar{x} = (x - x_I)/r_I$ and $\bar{y} = (y - y_I)/r_I$ where x_I and y_I are the horizontal and vertical center positions of the sphere I, respectively; $n = 1, 2, 3$.

Discretization	Local basis functions in 1D	Local basis functions in 2D
MFS-LIN	$\{1, \bar{x}\}$	$\{1, \bar{x}, \bar{y}, \bar{x}\bar{y}\}$
MFS-TRIn	$\left\{ \begin{matrix} 1, \bar{x}, \cos(\pi\bar{x}), \sin(\pi\bar{x}), \ldots, \\ \cos(n\pi\bar{x}), \sin(n\pi\bar{x}) \end{matrix} \right\}$	$\left\{ \begin{matrix} 1, \bar{x}, \bar{y}, \bar{x}\bar{y}, \\ \cos(\pi\bar{x}), \sin(\pi\bar{x}), \\ \cos(\pi\bar{y}), \sin(\pi\bar{y}), \\ \cos(\pi\bar{x} + \pi\bar{y}), \sin(\pi\bar{x} + \pi\bar{y}), \\ \cos(\pi\bar{x} - \pi\bar{y}), \sin(\pi\bar{x} - \pi\bar{y}), \ldots, \\ \cos(n\pi\bar{x}), \sin(n\pi\bar{x}), \\ \cos(n\pi\bar{y}), \sin(n\pi\bar{y}), \\ \cos(n\pi\bar{x} + n\pi\bar{y}), \sin(n\pi\bar{x} + n\pi\bar{y}), \\ \cos(n\pi\bar{x} - n\pi\bar{y}), \sin(n\pi\bar{x} - n\pi\bar{y}) \end{matrix} \right\}$

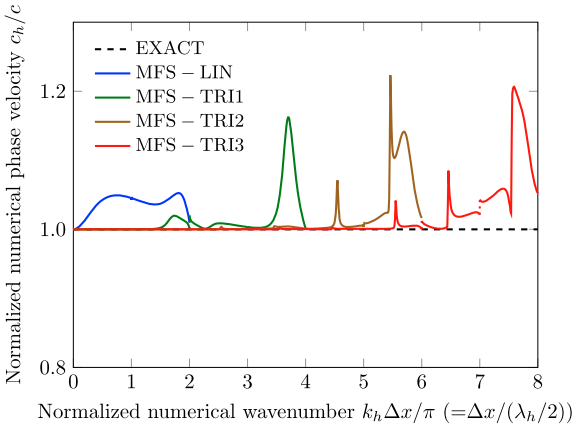

Fig. 2. Dispersion properties of the method of finite spheres in one-dimensional case: MFS-LIN, MFS-TRI1, MFS-TRI2 and MFS-TRI3 discretizations.

functions are used in each sphere I, i.e., $n_I = n_p$. We then assume the numerical sinusoidal plane wave solution to be of the form

$$\boldsymbol{\alpha} = \mathbf{A} e^{i(k_h \mathbf{n} \cdot \mathbf{x}_h - \omega_h t_h)} \tag{10}$$

where k_h, ω_h, $\mathbf{x}_h$ and t_h are the numerical wavenumber, the numerical angular frequency, the discretized position vector and the discretized time, respectively, and $\mathbf{A}$ is the amplitude vector with the components

$$\mathbf{A} = [A_1, A_2, \ldots, A_{n_p}, A_1, A_2, \ldots, A_{n_p}, \ldots]^{\mathrm{T}}. \tag{11}$$

Note that the local basis function set in each sphere has the same amplitude vector, i.e., the vector $[A_1, A_2, \ldots, A_{n_p}]^{\mathrm{T}}$ is repeated in Eq. (11).

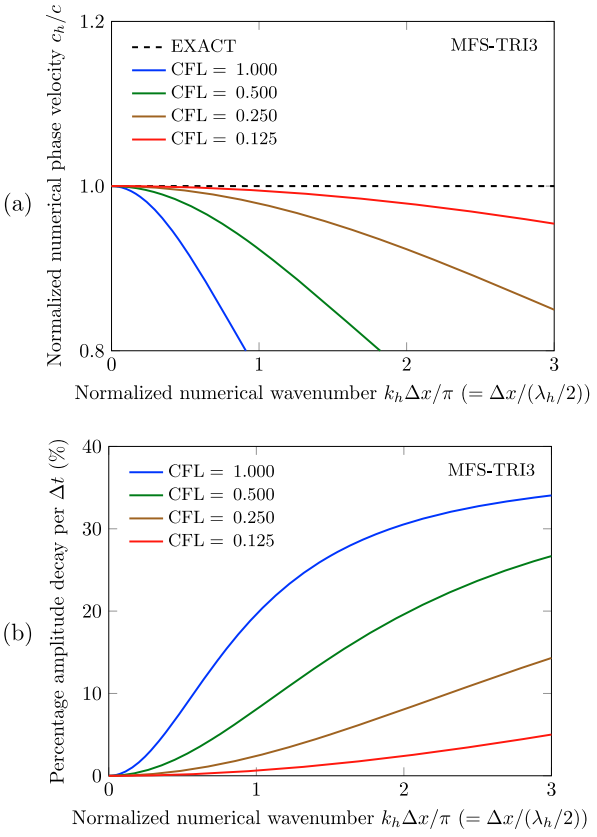

Fig. 4. Dispersion and dissipation properties of MFS-TRI3 scheme in one-dimensional case: (a) dispersion errors and (b) amplitude decays.

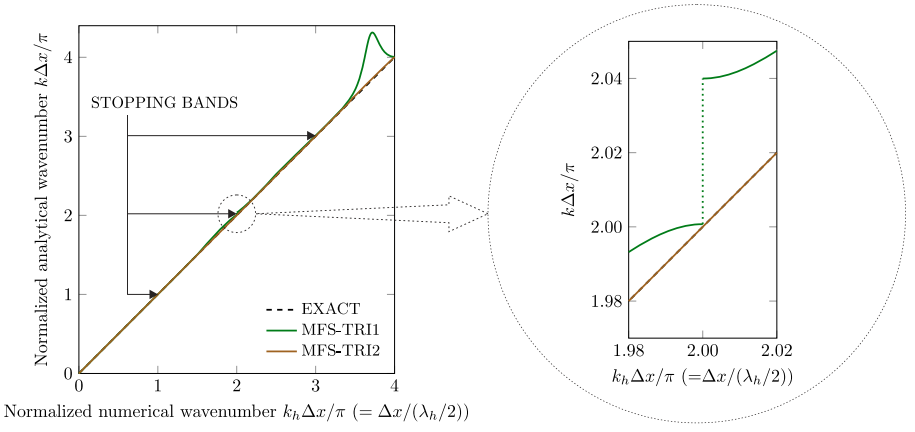

Fig. 3. Wavenumber spectrums and stopping bands of MFS-TRI1 and MFS-TRI2 discretizations.

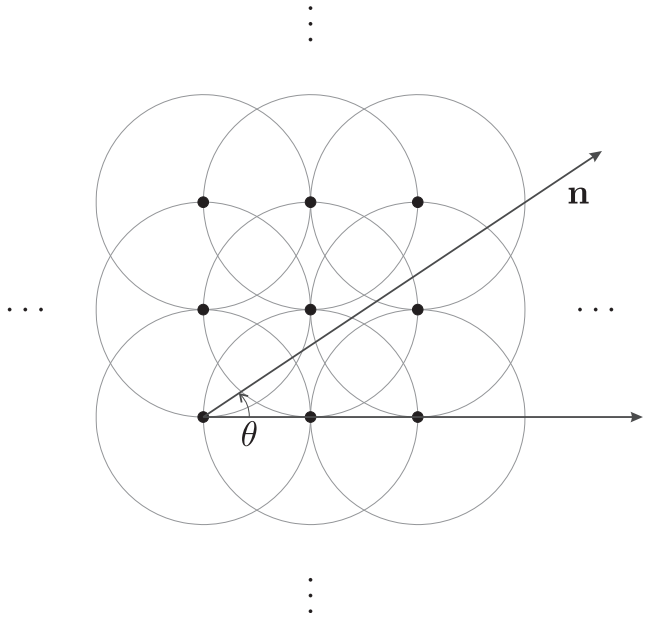

Fig. 5. Propagation angle of a sinusoidal plane wave.

If we substitute from Eq. (10) into Eq. (9), the same block equation with n_p unknowns is repeated, and the n'th block equation, which is associated with sphere n, is of the form, after canceling the common factor,

$$(\mathbf{D}_{\text{stiff}} - \lambda \mathbf{D}_{\text{mass}})\hat{\mathbf{A}} = \mathbf{0} \tag{12}$$

where $\mathbf{D}_{\text{stiff}}$ and $\mathbf{D}_{\text{mass}}$ are the corresponding resultant matrices, which are of order $n_p \times n_p$, $\hat{\mathbf{A}} = [A_1, A_2, \ldots, A_{n_p}]^{\mathrm{T}}$, and

$$\lambda = \frac{144[1 - \cos(\omega_h \Delta t/2)]}{\text{CFL}^2 \Delta x^2 [5 + 13\cos(\omega_h \Delta t/2) - i3\sin(\omega_h \Delta t/2)]} \tag{13}$$

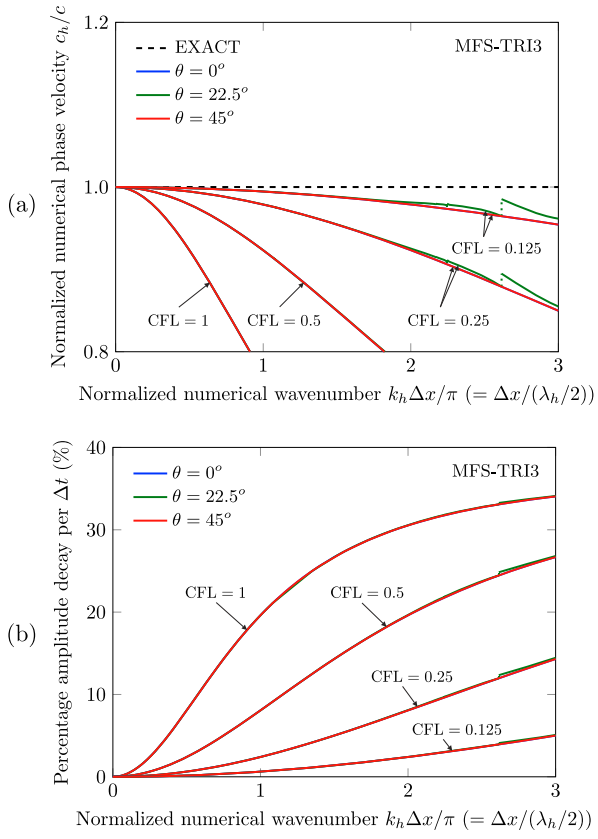

Fig. 7. Dispersion and dissipation properties of MFS-TRI3 scheme in two-dimensional case: (a) dispersion errors and (b) amplitude decays.

with $\text{CFL} = c\Delta t/\Delta x$. Note that ω_h is a complex number, the imaginary part of which is related to the amplitude decay, i.e.,

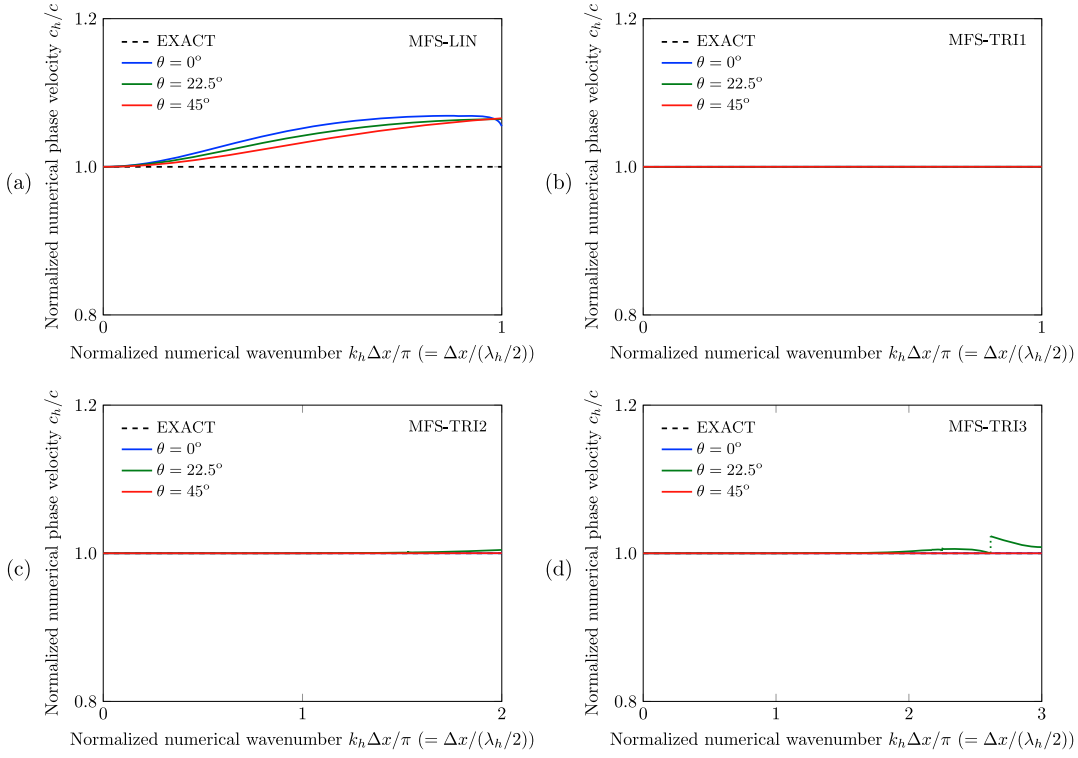

Fig. 6. Dispersion properties of the method of finite spheres in two-dimensional case: (a) MFS-LIN, (b) MFS-TRI1, (c) MFS-TRI2 and (d) MFS-TRI3 discretizations.

Percentage amplitude decay per Δt

$$= (1 - e^{\mathrm{Im}(\omega_h \Delta t)}) \times 100\%. \tag{14}$$

The existence of nontrivial solutions to Equation (12) requires

$$\det(\mathbf{D}_{\text{stiff}} - \lambda \mathbf{D}_{\text{mass}}) = 0. \tag{15}$$

The solution of the above equation provides the relation between the numerical wavenumber k_h and the numerical angular frequency ω_h depending on the CFL number, and in general the numerical phase velocity c_h $(= \omega_h / k_h)$ is not equal to the propagation velocity c, i.e., the numerical solution of the wave equation shows dispersion.

To obtain the dispersion error due only to the use of the method of finite spheres, we substitute from Eq. (10) into Eq. (8) with ω_h replaced by ω (also, t_h replaced by t). This procedure is equivalent to using Eq. (15) with $\Delta t \to 0$.

The dispersion properties, of course, depend on the local basis functions used in the method of finite spheres. In our mathematical analysis, we study different sets of local basis functions, i.e., the method of finite spheres with the bi-linear polynomials (MFS-LIN) and the method of finite spheres with the bi-linear polynomials and the trigonometric polynomials up to order n (MFS-TRIn, $n = 1, 2, 3$), as listed in Table 1.

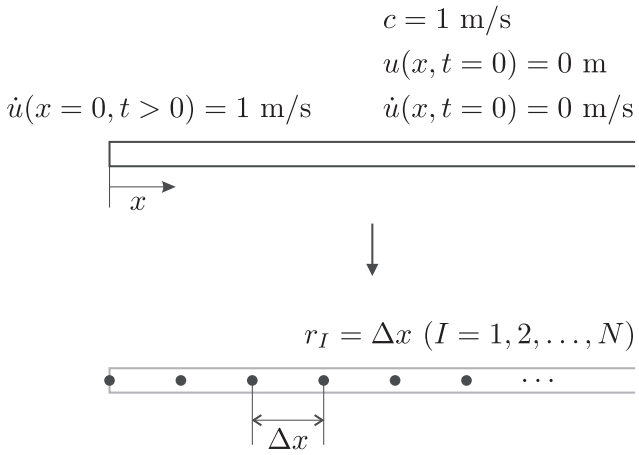

Fig. 8. 1D impact of an elastic bar problem: problem description and spatial discretization by finite spheres.

2.1. Dispersion properties in 1D case

In the one-dimensional case, the matrices $\mathbf{D}_{\text{stiff}}$ and $\mathbf{D}_{\text{mass}}$ are

$$\mathbf{D}_{\text{stiff}} = \mathbf{K}_{n,n-1} e^{-ik_h \Delta x} + \mathbf{K}_{n,n} + \mathbf{K}_{n,n+1} e^{ik_h \Delta x} \tag{16}$$

and

$$\mathbf{D}_{\text{mass}} = \mathbf{M}_{n,n-1} e^{-ik_h \Delta x} + \mathbf{M}_{n,n} + \mathbf{M}_{n,n+1} e^{ik_h \Delta x}. \tag{17}$$

In the above equations, the stiffness matrix $\mathbf{K}_{n,n+k}$ and the mass matrix $\mathbf{M}_{n,n+k}$ are sub-matrices of the total stiffness and mass matrices defined in Eq. (9), respectively, and the subscript $n+k$ $(k = -1, 0, 1)$ means the associated sphere $n+k$, see Fig. 1(a).

Fig. 2 shows the dispersion error induced by the spatial discretizations only, MFS-LIN and MFS-TRIn (here, $n = 1, 2, 3$), as a function of the normalized numerical wavenumber $k_h \Delta x / \pi$ $(= \Delta x / (\lambda_h / 2)$ where λ_h is the numerical wavelength). Here, since temporal discretization is not considered, the vertical axis is actually the ratio of the exact wavenumber k to the numerical wavenumber k_h, i.e., $c_h / c = k / k_h$. Two valuable properties of the method of finite spheres solutions are observed in Figs. 2 and 3. First, there are stopping bands, jumps in the values of the normalized numerical phase velocity, plotted as dotted vertical lines in Figs. 2 and 3. In these bands, the corresponding numerical wavenumber is a complex number, which means that the corresponding wave modes decay. For the MFS-TRIn discretizations,

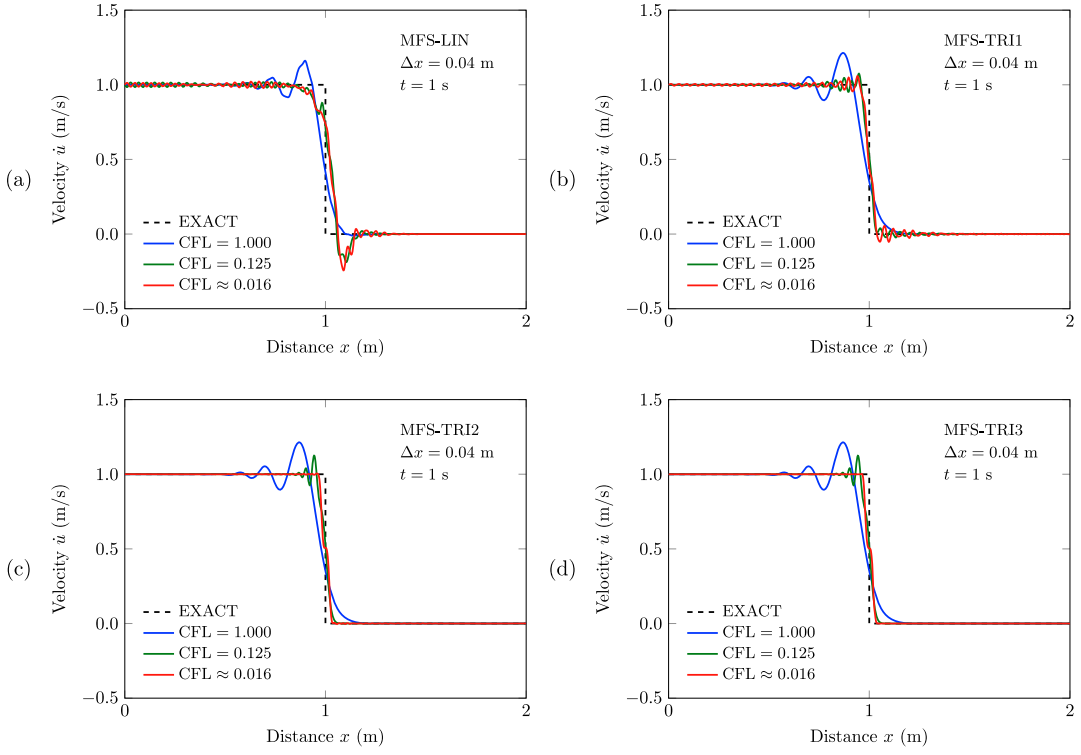

Fig. 9. Velocity distributions of the bar at $t = 1$ s when decreasing the CFL number: using (a) MFS-LIN, (b) MFS-TRI1, (c) MFS-TRI2 and (d) MFS-TRI3 schemes, with 51 spheres.

the magnitude of stopping bands in lower wavenumber regions decreases as the order of trigonometric polynomials n increases. For example, the magnitude of a stopping band corresponding to $k_h\Delta x/\pi = 2$ drops to almost zero as the order n increases from 1 to 2, see Fig. 3. Second, most importantly, the MFS-TRIn discretizations have almost no dispersion for $0 \leqslant k_h\Delta x/\pi \leqslant n$. In other words, the solutions to the Helmholtz equation are very accurately calculated by the MFS-TRIn discretizations up to the wave mode with $k_h\Delta x/\pi = n$. This property is consistent with the fact that the method of finite spheres can exactly reproduce the function used in the basis [24].

Since the MFS-TRIn discretizations introduce negligible dispersion error for sinusoidal waves with $k_h\Delta x/\pi \in [0, n]$, the dispersion error of these wave modes is entirely related to the time integration method used, which is in this study the Bathe method. Fig. 4 shows the dispersion errors and the percentage amplitude decays of wave modes with $k_h\Delta x/\pi \in [0, 3]$ when using the MFS-TRI3 discretization and the Bathe method. We observe that a decrease in the CFL number results in a decrease in both the dispersion error and the amplitude decay, i.e., more accurate solutions. This property implies that for wave modes with $k_h\Delta x/\pi \in [0, n]$, the MFS-TRI$n$ schemes do not require an optimal CFL number which gives the best solution, i.e., more accurate solutions are obtained monotonically by decreasing the CFL number.

The wave modes with $k_h\Delta x/\pi > n$ are damped out in practical analyses since in practice we do not use a very small CFL number

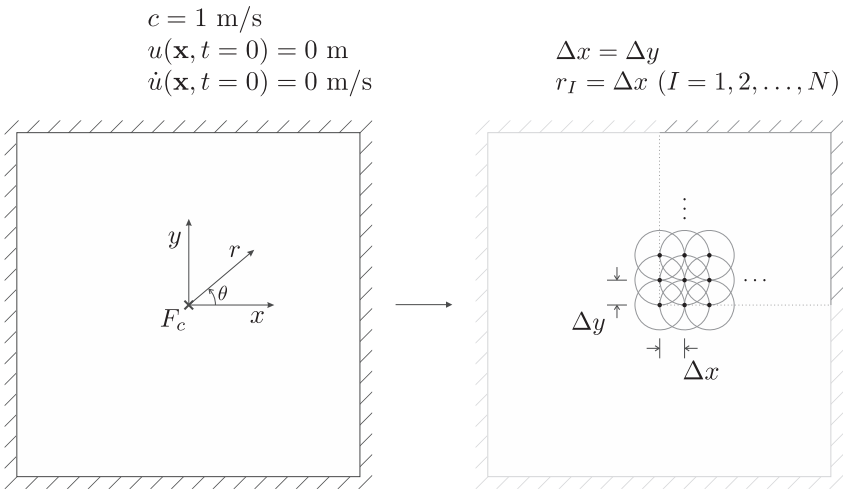

Fig. 10. 2D scalar wave propagation in a pre-stressed membrane: problem description and spatial discretization by finite spheres.

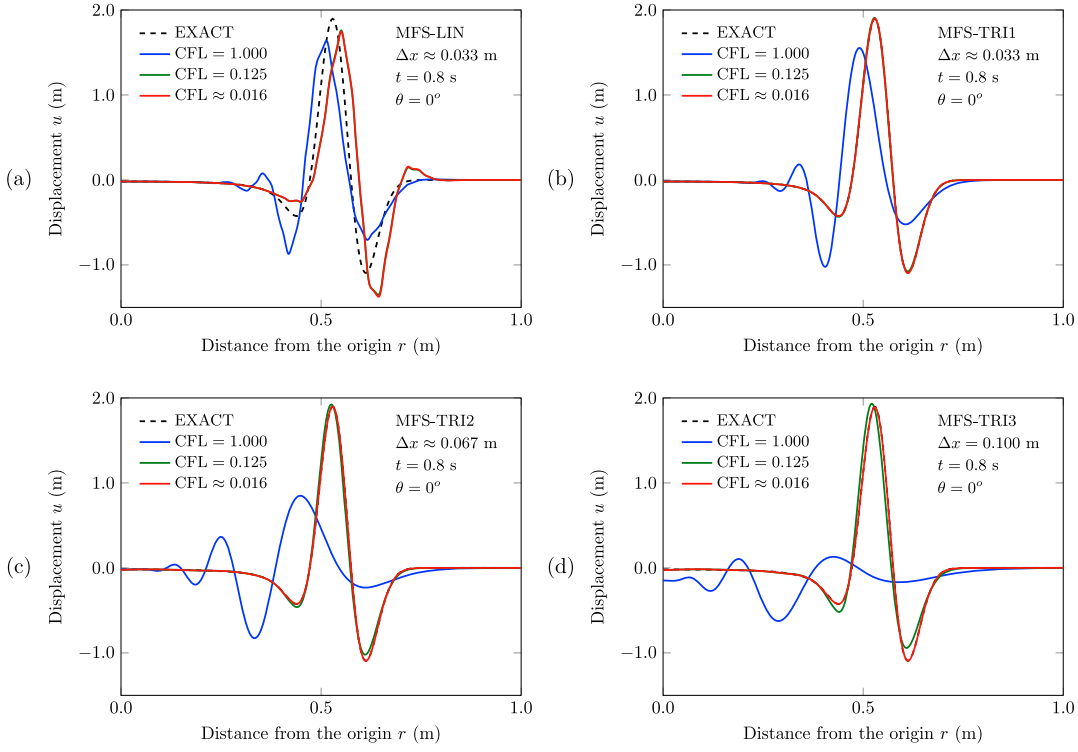

Fig. 11. Displacement distributions of the membrane along horizontal axis ($\theta = 0^o$) at $t = 0.8$ s when decreasing the CFL number: using (a) MFS-LIN scheme with 31×31 spheres, (b) MFS-TRI1 scheme with 31×31 spheres, (c) MFS-TRI2 scheme with 16×16 spheres and (d) MFS-TRI3 scheme with 11×11 spheres.

for these modes. Note that the amplitude decay depends on the CFL number and the normalized numerical wavenumber and an increase in the CFL number or in the normalized numerical wavenumber leads to an increase in the amplitude decay, see Fig. 4(b).

2.2. Dispersion properties in 2D case

In the two-dimensional case, we obtain

$$\begin{aligned}\mathbf{D}_{\text{stiff}} = {} & \mathbf{K}_{n,n} + \mathbf{K}_{n,n-1}e^{-ik_h\Delta x\cos\theta} + \mathbf{K}_{n,n+1}e^{ik_h\Delta x\cos\theta} \\ & + \mathbf{K}_{n,n-2}e^{ik_h\Delta x(\cos\theta-\sin\theta)} + \mathbf{K}_{n,n+2}e^{ik_h\Delta x(-\cos\theta+\sin\theta)} \\ & + \mathbf{K}_{n,n-3}e^{-ik_h\Delta x\sin\theta} + \mathbf{K}_{n,n+3}e^{ik_h\Delta x\sin\theta} \\ & + \mathbf{K}_{n,n-4}e^{-ik_h\Delta x(\cos\theta+\sin\theta)} + \mathbf{K}_{n,n+4}e^{ik_h\Delta x(\cos\theta+\sin\theta)} \end{aligned} \tag{18}$$

and

$$\begin{aligned}\mathbf{D}_{\text{mass}} = {} & \mathbf{M}_{n,n} + \mathbf{M}_{n,n-1}e^{-ik_h\Delta x\cos\theta} + \mathbf{M}_{n,n+1}e^{ik_h\Delta x\cos\theta} \\ & + \mathbf{M}_{n,n-2}e^{ik_h\Delta x(\cos\theta-\sin\theta)} + \mathbf{M}_{n,n+2}e^{ik_h\Delta x(-\cos\theta+\sin\theta)} \\ & + \mathbf{M}_{n,n-3}e^{-ik_h\Delta x\sin\theta} + \mathbf{M}_{n,n+3}e^{ik_h\Delta x\sin\theta} \\ & + \mathbf{M}_{n,n-4}e^{-ik_h\Delta x(\cos\theta+\sin\theta)} + \mathbf{M}_{n,n+4}e^{ik_h\Delta x(\cos\theta+\sin\theta)} \end{aligned} \tag{19}$$

where θ is the angle between the direction of wave propagation and the horizontal axis of the Cartesian coordinate system, as shown in Fig. 5. As in the one-dimensional case, the subscript $n+k$ ($k=-4,-3,\ldots,3,4$) in the above equations denotes the associated sphere $n+k$, see Fig. 1(b).

The dispersion properties of the method of finite spheres due to the spatial discretizations only in the two-dimensional case are very similar to those in the one-dimensional case, i.e., for the MFS-TRI*n* discretizations (here, $n=1,2,3$), wave modes with $k_h\Delta x/\pi \in [0,n]$ are almost non-dispersive, as shown in Fig. 6. Another important point to note is that the numerical anisotropy is negligible in these wave modes. This property is clearly seen in Figs. 6 and 7 where the results of a MFS-TRI*n* scheme for different angles θ are approximately the same.

From the above results, it can be concluded that if Δx is chosen such that the response is well approximated by wave modes with $k_h\Delta x/\pi \in [0,n]$ and the contributions of wave modes with $k_h\Delta x/\pi > n$ can be neglected, the MFS-TRI*n* schemes give more accurate solutions with negligible numerical anisotropy as the CFL number decreases.

3. Numerical examples

Our objective in this section is to illustrate through numerical examples that the solutions of wave propagation problems using the MFS-TRI*n* discretizations ($n=1,2,3$) with the Bathe method converge to the exact analytical solutions when decreasing the CFL number and are almost independent of the propagation direction if we choose Δx such that the wave modes with $0 \leqslant k_h\Delta x/\pi \leqslant n$ are sufficient to accurately approximate the response. We first consider scalar wave propagations in one- and two-dimensional media and then solve the Lamb's problem [29], where we have different types of wave propagations in a semi-infinite elastic medium. These examples are taken from Refs. [1,9,19].

In all numerical examples, the computational domain is sufficiently large so that a wave does not reach the boundary of the computational domain for the time considered. We do not employ, therefore, a technique such as a perfectly matched layer [30–33] to suppress artificially reflected waves at the boundary of the computational domain. For the discretization, like in the dispersion analyses, we uniformly distribute spheres with $r_I = \Delta x$ and use the Bathe method.

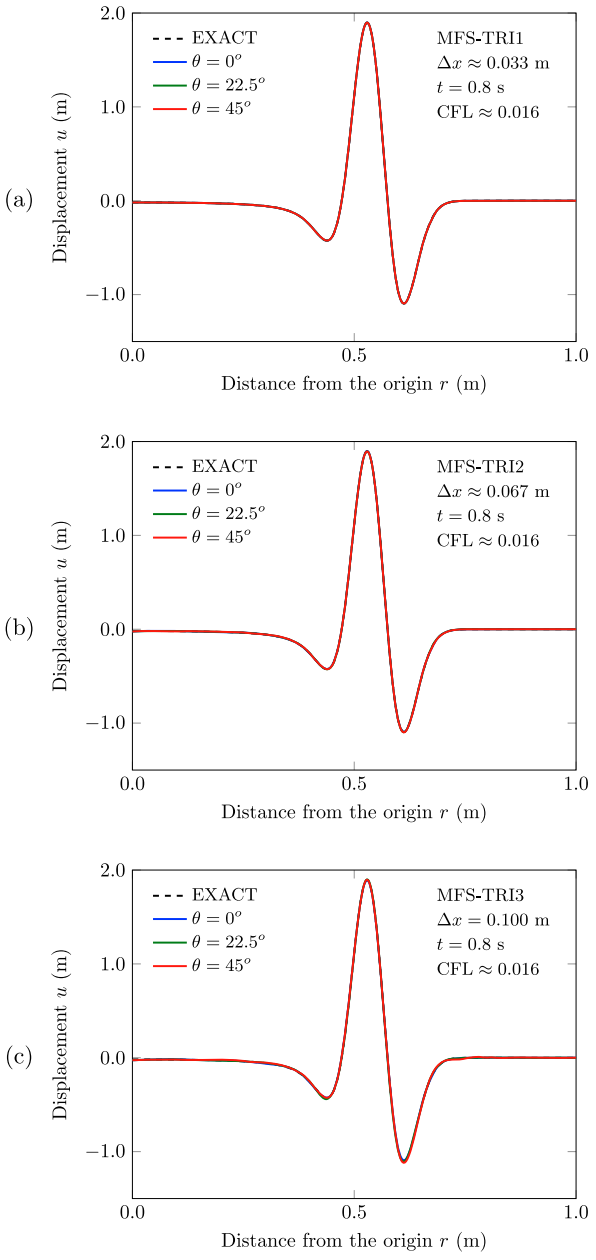

Fig. 12. Displacement distributions of the membrane along various directions ($\theta = 0°, 22.5°, 45°$) at $t = 0.8$ s: when using (a) MFS-TRI1 scheme with 31×31 spheres, (b) MFS-TRI2 scheme with 16×16 spheres and (c) MFS-TRI3 scheme with 11×11 spheres; CFL ≈ 0.016.

The computational expense of obtaining two-dimensional scalar wave solutions when using the MFS-TRI*n* discretizations with the Bathe method was studied to some degree in Ref. [1] where it was observed that for approximately the same relative error measured in the L^2 norm, the computational times used in the MFS-TRI*n* schemes are close to the times used for the bi-linear finite element solutions. The reason for this observation is that using the MFS-TRI*n* schemes a relatively coarse spatial discretization with a similar time step size can be used. The major effort in all solution procedures then pertains to the vector forward reductions and back-substitutions in the time integrations since the evaluations of the stiffness and mass matrices and the matrix factorizations are performed only once. However, since we considered

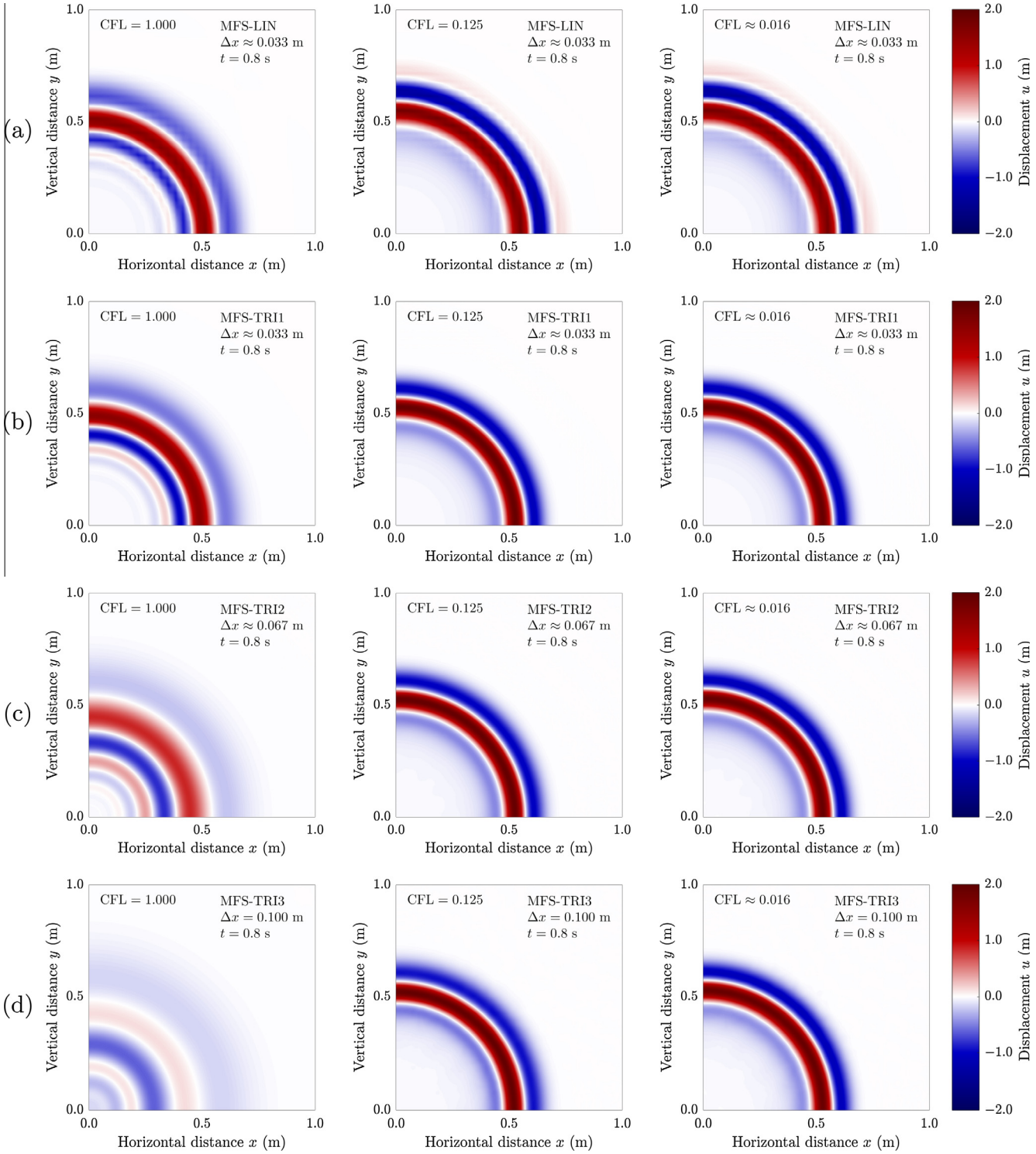

Fig. 13. Snapshots of displacement distributions of the membrane at $t = 0.8$ s when decreasing the CFL number: using (a) MFS-LIN scheme with 31×31 spheres, (b) MFS-TRI1 scheme with 31×31 spheres, (c) MFS-TRI2 scheme with 16×16 spheres and (d) MFS-TRI3 scheme with 11×11 spheres.

only the solutions of two-dimensional academic problems, a detailed study of various cases in engineering practice, including three-dimensional response solutions, would be valuable.

3.1. 1D impact of an elastic bar

We consider the one-dimensional wave propagation due to an impact on an elastic semi-infinite bar, as shown in Fig. 8. The governing equation for the displacement u of the bar is the one-dimensional wave equation (Eq. (1) in 1D) where $c = 1$ m/s. All initial conditions are zero and a unit step velocity is applied at the left end, see Fig. 8.

To solve this problem, we calculate all solutions with $\Delta x = 0.04$ m, which corresponds to the number of spheres $N = 51$ for the computational domain $V = [0, 2]$, see Fig. 8. Fig. 9 shows the results obtained. We see that with the different MFS-TRI*n* schemes we obtain similar results when CFL $= 1$, and that the solutions are monotonically improved when using the MFS-TRI*n*

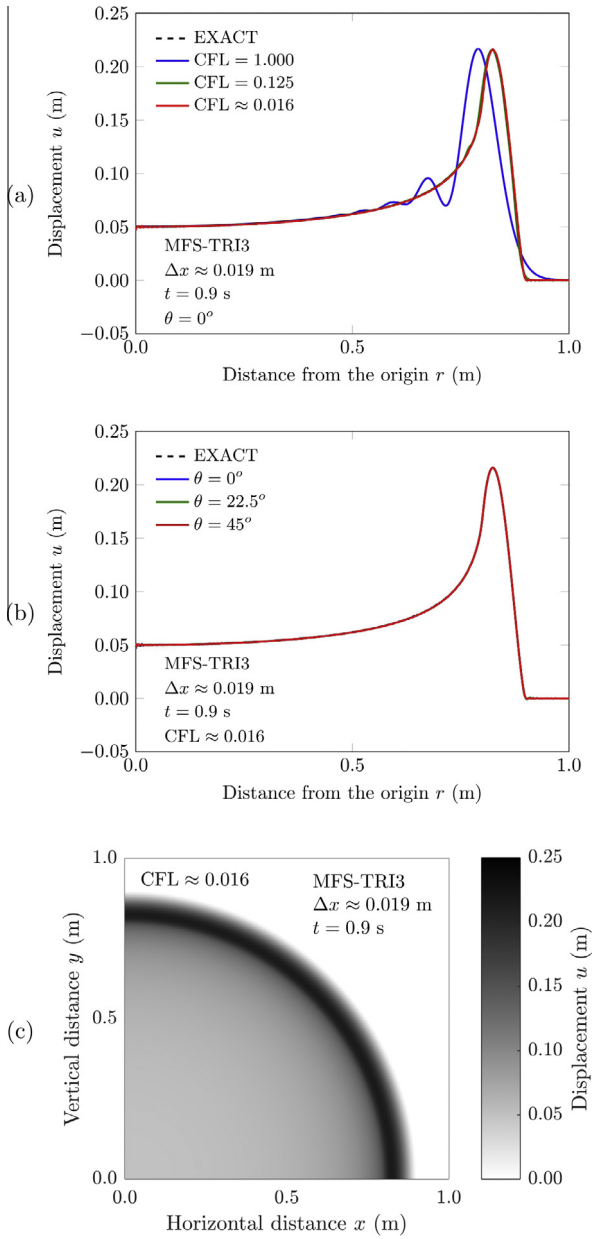

Fig. 14. Displacement distributions of the membrane at $t = 0.9$ s when using MFS-TRI3 scheme with 55×55 spheres: (a) displacement distributions along horizontal axis with decreasing the CFL number, (b) displacement distributions along various directions ($\theta = 0°, 22.5°, 45°$) when CFL ≈ 0.016 and (c) snapshot of displacement distributions when CFL ≈ 0.016.

schemes by decreasing the CFL number. Using the MFS-TRI2 and MFS-TRI3 schemes surprisingly accurate results are obtained when a small CFL number is used. A more accurate solution with the MFS-TRI1 scheme can be obtained by increasing the number of spheres, i.e. decreasing the value of Δx.

3.2. 2D scalar wave propagation

We next consider the two-dimensional scalar wave propagation resulting from a concentrated force (a point excitation) F_c applied at the center of a pre-stressed square membrane as described in Fig. 10. The displacement of the membrane u is governed by the two-dimensional wave equation (Eq. (1) in 2D) where $c = 1$ m/s. The membrane is initially at rest and for the computation only the domain $V = [0, 1] \times [0, 1]$ is considered, because of symmetry.

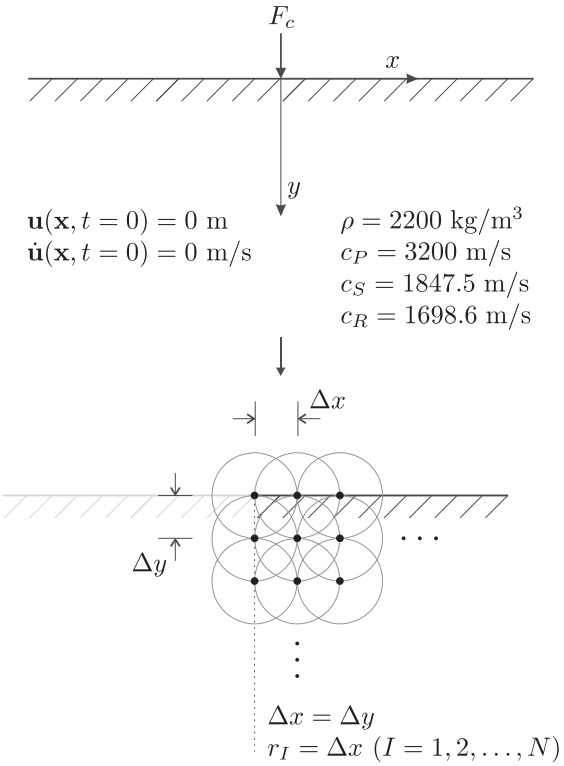

Fig. 15. The Lamb's problem [29] - 2D wave propagation in a plane strain elastic half-space: problem description and spatial discretization by finite spheres.

First, a Ricker wavelet is considered as the concentrated force

$$F_c = A_F[1 - 2\pi^2 f_p^2 (t - t_s)^2] e^{-\pi^2 f_p^2 (t - t_s)^2} \tag{20}$$

where A_F is the amplitude of the force, f_p is the peak frequency and t_s is the time shift. In this problem, we use $A_F = 40$ m/s^2, $f_p = 5$ Hz and $t_s = 0.25$ s. The solutions are computed using the schemes MFS-LIN with 31×31 spheres, MFS-TRI1 with 31×31 spheres, MFS-TRI2 with 16×16 spheres and MFS-TRI3 with 11×11 spheres. Fig. 11 shows the calculated displacements along the horizontal axis at $t = 0.8$ s. We observe that while the MFS-LIN scheme does not give an accurate solution, the solutions of MFS-TRIn converge to the exact solution as the CFL number decreases. Another important observation is that the accuracy of these solutions is almost the same for any angle θ considered, see Figs. 12 and 13.

Next we consider the wave propagation due to a concentrated force

$$F_c = \begin{cases} 1.6 \times 10^3 t(0.1 - t) & \text{for } 0 \leqslant t < 0.1, \\ 0 & \text{for } t \geqslant 0.1. \end{cases} \tag{21}$$

Since much higher wave modes need now be captured to predict the response accurately we use 55×55 spheres for the MFS-TRI3 scheme. Fig. 14 shows the results at $t = 0.9$ s, namely, the displacement distributions along the horizontal axis with decreasing the CFL number, the displacement distributions along three different directions when CFL ≈ 0.016, and the overall displacement distributions in the computational domain when CFL ≈ 0.016. As in the previous case, a more accurate solution is obtained when decreasing the CFL number and the solution accuracy is almost independent of θ.

3.3. 2D elastic wave propagation

In this solution we consider two-dimensional waves propagating in a semi-infinite elastic medium in plane strain conditions

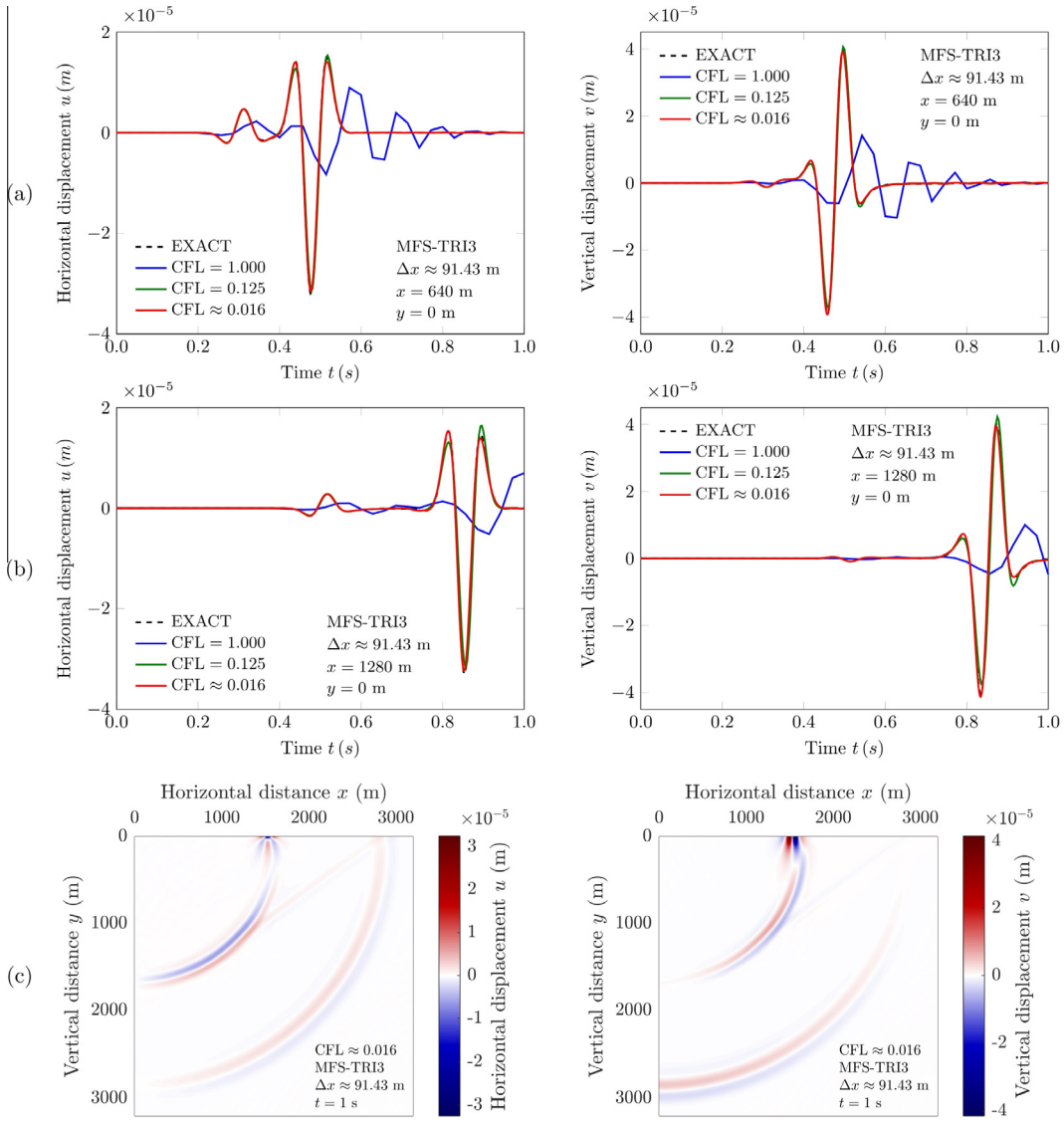

Fig. 16. Horizontal and vertical displacements of the elastic medium when using MFS-TRI3 scheme with 36×36 spheres: (a) displacement histories at $\mathbf{x} = (640, 0)$ m with decreasing the CFL number, (b) displacement histories at $\mathbf{x} = (1280, 0)$ m with decreasing the CFL number and (c) snapshots of displacement distributions at $t = 1$ s when CFL ≈ 0.016.

[29], as illustrated in Fig. 15. The concentrated line force located at the free surface of the medium is a Ricker wavelet, see Equation (20), with $A_F = 2 \times 10^6$ N/m, $f_p = 10$ Hz and $t_s = 0.1$ s. For the material properties, we use the mass density $\rho = 2200$ kg/m^3, the P-wave velocity $c_P = 3200$ m/s and the S-wave velocity $c_S = 1847.5$ m/s, which gives the Rayleigh wave velocity $c_R \approx 1698.6$ m/s. The initial displacements and velocities are zero and the computational domain $V = [0, 3200] \times [0, 3200]$ is considered. The displacements $\mathbf{u} = [u, v]^{\mathrm{T}}$ of the medium are governed by the Navier equations, which can be expressed in the form of wave equations by the Helmholtz decomposition [34].

We use the MFS-TRI3 scheme with 36×36 spheres for the solution and calculate the time step size Δt based on the P-wave velocity because then the other types of waves are also accurately simulated, indeed more accurately. Fig. 16 shows the predicted horizontal and vertical displacements, namely the calculated displacement histories at two receivers located at $\mathbf{x} = (640, 0)$ m and at $\mathbf{x} = (1280, 0)$ m with decreasing the CFL number, and the overall displacement distributions in the computational domain at $t = 1$ s when CFL ≈ 0.016. As expected, the numerical solutions of all three waves monotonically converge to the exact solutions as the CFL number is decreased.

4. Concluding remarks

The objective in this paper was to present a study of the method of finite spheres used with the Bathe method for time integration in the solution of transient wave propagation problems. We analyzed the dispersion property of the method of finite spheres and the numerical effects introduced when using the Bathe method. We illustrated these properties through the solutions of numerical examples. Although we considered only one- and two-dimensional cases, the same analysis can be extended to the three-dimensional case.

The key observation is that we can use the method of finite spheres with the bi-linear polynomials and the trigonometric polynomials as local basis functions to calculate the solution with increasing accuracy as the CFL number is decreased. This is most important and in contrast to the use of the traditional finite elements. Hence very accurate solutions can be obtained when

multiple types of waves at different speeds propagate by using the largest wave speed to select the CFL number. Indeed any speed can be chosen for the CFL number if it is larger than all wave speeds. Furthermore, with the uniform sphere arrangements used, the solutions of the problems considered in this paper were accurate in any direction.

However, we only considered uniformly distributed spheres of the same radius and only one time integration method. It would be of value to investigate the performance of the method of finite spheres when non-uniform distributions of spheres with different radii are used and when different time integration methods are employed. Also, three-dimensional solutions should be considered [35]. Furthermore, a detailed study of discretizations based on coupling traditional finite elements with the method of finite spheres, as proposed in Ref. [36], for accurate dynamic analyses would be valuable.

References

[1] Ham S, Lai B, Bathe KJ. The method of finite spheres for wave propagation problems. Comput Struct 2014;142:1–14.
[2] Krieg RD, Key SW. Transient shell response by numerical time integration. Int J Numer Meth Eng 1973;7:273–86.
[3] Belytschko T, Mullen R. On dispersive properties of finite element solutions. In: Miklowitz J, Achenbach JD, editors. Modern problems in elastic wave propagation. New York (NY): Wiley; 1978. p. 67–82.
[4] Mullen R, Belytschko T. Dispersion analysis of finite element semidiscretizations of the two-dimensional wave equation. Int J Numer Meth Eng 1982;18:11–29.
[5] Marfurt KJ. Accuracy of finite-difference and finite-element modeling of the scalar and elastic wave equations. Geophysics 1984;49:533–49.
[6] Abboud NN, Pinsky PM. Finite element dispersion analysis for the three-dimensional second-order scalar wave equation. Int J Numer Meth Eng 1992;35:1183–218.
[7] Thompson LL, Pinsky PM. Complex wavenumber Fourier analysis of the *p*-version finite element method. Comput Mech 1994;13:255–75.
[8] Deraemaeker A, Babuška I, Bouillard P. Dispersion and pollution of the FEM solution for the Helmholtz equation in one, two and three dimensions. Int J Numer Meth Eng 1999;46:471–99.
[9] Noh G, Ham S, Bathe KJ. Performance of an implicit time integration scheme in the analysis of wave propagations. Comput Struct 2013;123:93–105.
[10] Christon MA. The influence of the mass matrix on the dispersive nature of the semi-discrete, second-order wave equation. Comput Methods Appl Mech Eng 1999;173:147–66.
[11] Bathe KJ, Noh G. Insight into an implicit time integration scheme for structural dynamics. Comput Struct 2012;98–99:1–6.
[12] Bathe KJ. Finite element procedures. 2nd ed. Watertown (MA): Klaus-Jürgen Bathe; 2014.
[13] Guddati MN, Yue B. Modified integration rules for reducing dispersion error in finite element methods. Comput Methods Appl Mech Eng 2004;193:275–87.
[14] Idesman AV, Schmidt M, Foley JR. Accurate finite element modeling of linear elastodynamics problems with the reduced dispersion error. Comput Mech 2011;47:555–72.
[15] Thompson LL, Pinsky PM. A Galerkin least-squares finite element method for the two-dimensional Helmholtz equation. Int J Numer Meth Eng 1995;38:371–97.
[16] Babuška I, Ihlenburg F, Paik ET, Sauter SA. A generalized Finite Element Method for solving the Helmholtz equation in two dimensions with minimal pollution. Comput Methods Appl Mech Eng 1995;128:325–59.
[17] Franca LP, Farhat C, Macedo AP, Lesoinne M. Residual-free bubbles for the Helmholtz equation. Int J Numer Meth Eng 1997;40:4003–9.
[18] Kohno H, Bathe KJ, Wright JC. A finite element procedure for multiscale wave equations with application to plasma waves. Comput Struct 2010;88:87–94.
[19] Ham S, Bathe KJ. A finite element method enriched for wave propagation problems. Comput Struct 2012;94–95:1–12.
[20] Patera AT. A spectral element method for fluid dynamics: laminar flow in a channel expansion. J Comput Phys 1984;54:468–88.
[21] Seriani G, Oliveira SP. Dispersion analysis of spectral element methods for elastic wave propagation. Wave Motion 2008;45:729–44.
[22] Bathe KJ, Baig MMI. On a composite implicit time integration procedure for nonlinear dynamics. Comput Struct 2005;83:2513–24.
[23] Bathe KJ. Conserving energy and momentum in nonlinear dynamics: a simple implicit time integration scheme. Comput Struct 2007;85:437–45.
[24] De S, Bathe KJ. The method of finite spheres. Comput Mech 2000;25:329–45.
[25] De S, Bathe KJ. Displacement/pressure mixed interpolation in the method of finite spheres. Int J Numer Meth Eng 2001;51:275–92.
[26] De S, Bathe KJ. The method of finite spheres with improved numerical integration. Comput Struct 2001;79:2183–96.
[27] De S, Bathe KJ. Towards an efficient meshless computational technique: the method of finite spheres. Eng Comput 2001;18:170–92.
[28] Shepard D. A two-dimensional interpolation function for irregularly-spaced data. In: Proceedings of the 1968 23rd ACM national conference. New York (NY, USA): ACM; 1968. p. 517–24.
[29] Lamb H. On the propagation of tremors over the surface of an elastic solid. Philos Trans Roy Soc Lond. Ser A, Contain Pap Math Phys Charact 1904;203:1–42.
[30] Berenger JP. A perfectly matched layer for the absorption of electromagnetic waves. J Comput Phys 1994;114:185–200.
[31] Chew WC, Weedon WH. A 3D perfectly matched medium from modified Maxwell's equations with stretched coordinates. Microwave Opt Technol Lett 1994;7:599–604.
[32] Teixeira FL, Chew WC. General closed-form PML constitutive tensors to match arbitrary bianisotropic and dispersive linear media. IEEE Microwave Guided Wave Lett 1998;8:223–5.
[33] Sacks ZS, Kingsland DM, Lee R, Lee JF. A perfectly matched anisotropic absorber for use as an absorbing boundary condition. IEEE Trans Antennas Propag 1995;43:1460–3.
[34] Achenbach JD. Wave propagation in elastic solids. Amsterdam (The Netherlands): North-Holland Publishing Company; 1973.
[35] Lai B, Bathe KJ. The method of finite spheres in three-dimensional static analysis. Comput Struct 2016;173:161–73.
[36] Bathe KJ, Zhang L. The finite element method with overlapping elements – a new paradigm for CAD driven simulations, in preparation.